

# Addressing the Hubble Tension: Insights from Reversible and Irreversible Thermodynamic Processes

Hussain Gohar<sup>1, a</sup>

<sup>1</sup>*Institute of Physics, University of Szczecin, Wielkopolska 15, 70-451 Szczecin, Poland*

(Dated: July 9, 2025)

We investigate the role of reversible and irreversible thermodynamic processes in a cosmological context, focusing on their impact on the early and late-time expansion history of the universe. In our framework, gravitationally induced adiabatic matter creation/annihilation are treated as irreversible processes, while energy exchange between the cosmic bulk and the horizon is modeled as reversible. We propose two thermodynamic interacting scenarios with matter creation/annihilation in which energy flows from matter and radiation components to an effective entropic dark energy sector. In both scenarios, effective entropic dark energy initially exhibits properties akin to those of radiation and matter prior to recombination. Subsequently, it transitions into a quintessence state, ultimately converging towards the cosmological constant in the current epoch. Our models predict Hubble constant values of  $H_0 = 71.73 \pm 0.79 \text{ km s}^{-1} \text{ Mpc}^{-1}$  and  $H_0 = 71.06 \pm 0.79 \text{ km s}^{-1} \text{ Mpc}^{-1}$ , which exhibit agreement with the recent 2024 SH0ES measurement of  $H_0 = 73.17 \pm 0.86 \text{ km s}^{-1} \text{ Mpc}^{-1}$  at levels of  $1.2\sigma$  and  $1.8\sigma$ . When compared to the 2022 SH0ES baseline measurement of  $H_0 = 73.04 \pm 1.04 \text{ km s}^{-1} \text{ Mpc}^{-1}$ , both models demonstrate concordance at  $1\sigma$  and  $1.5\sigma$ . These results demonstrate that such thermodynamically motivated interactions can address the Hubble tension within a minimal extension of the standard cosmological model.

## I. INTRODUCTION

The Lambda Cold Dark Matter ( $\Lambda$ CDM) model provides a robust explanation for the accelerated expansion of the universe and aligns with high-precision observational data [1–8]. However, it faces several theoretical and observational challenges [9–11], most notably its inability to elucidate the origins of dark energy [12–14] and dark matter [15, 16]. From a data-centric viewpoint, the principal issue lies in the prediction of the current value of the Hubble parameter  $H_0$  by  $\Lambda$ CDM using cosmic microwave background (CMB) data [4] compared to direct observations of  $H_0$  from SH0ES [17–19]. The discrepancy first surfaced with Planck satellite data, highlighting a mismatch between the base  $\Lambda$ CDM estimation of  $H_0$  and the evaluation of the Cepheid distance ladder by the SH0ES collaboration. This *Hubble tension* has intensified as SH0ES' recent measurements [19] show  $H_0 = 73.17 \pm 0.86 \text{ km s}^{-1} \text{ Mpc}^{-1}$ , which is  $5.8\sigma$  above Planck's base  $\Lambda$ CDM value of  $H_0 = 67.4 \pm 0.5 \text{ km s}^{-1} \text{ Mpc}^{-1}$ . A wide variety of solutions have been proposed to address this tension [20–24]. Among them are holographic dark energy models [25], dynamical dark energy models [26], interacting dark energy models [27, 28], and early dark energy models [29, 30], among others. Reference [22] presents a systematic classification of these solutions according to how well they resolve the  $H_0$  tension combining different data sets, taking into account the  $1\sigma$ ,  $2\sigma$ , and  $3\sigma$  confidence levels. An approach to addressing the *Hubble tension* involves altering the post-recombination expansion history to raise the  $H_0$  value, termed as *late time solutions*. Contrarily, *early time solutions* modify

the expansion history before recombination, thereby adjusting  $H_0$  to resolve the tension.

In this article, we investigate a new way to address the *Hubble tension* by considering thermodynamic reversible and irreversible processes to the energy momentum tensor. These modifications change the energy-momentum tensor of the perfect fluid by incorporating additional terms coming from the gravitationally induced adiabatic creation/annihilation of matter (irreversible process) and the energy exchange between the bulk and the cosmological horizon (reversible process). As a result, the Friedmann, acceleration, and continuity equations are modified, and these changes are responsible for the present accelerated expansion of the universe. Furthermore, these modifications provide a promising way to address the *Hubble tension*.

Thermodynamic processes, encompassing both reversible and irreversible, hold a pivotal role within cosmology. Irreversible processes were initially introduced to the cosmological framework by Prigogine et al. [31] and have subsequently been employed to describe both the universe's early and late-time accelerated expansion phases of the universe [32–47]. These processes entail the adiabatic creation of matter, culminating in the generation of irreversible entropy. The mechanism of energy exchange, construed as a reversible process, between the universe's bulk and its cosmological horizon is intrinsically rooted in the holographic principle, which interrelates entropy, temperature, and energy with the horizon, indicating a reversible modality of energy transfer. Foundational investigations, including [48–55], have examined phenomena such as vacuum decay and fluid interactions. This study endeavors to integrate both reversible and irreversible processes to deepen the comprehension of the universe's evolution.

The functions pertaining to the rate of matter cre-

<sup>a</sup> [hussain.gohar@usz.edu.pl](mailto:hussain.gohar@usz.edu.pl)

ation and the entropy of the horizon, with the respective horizon temperature, are integral to our analysis. Nonetheless, the exact mechanisms underpinning gravitational particle production remain inadequately comprehended within the framework of quantum field theory [56–58]. We employ a specific phenomenological function for matter creation rates; for considerations of other general phenomenological functions, see [44, 47]. In relation to the flow of energy, we utilize the conventional Hawking temperature alongside our recently introduced generalized horizon entropy [59]. We outline scenarios of matter creation and energy flow across the horizon, thereby formulating distinct cosmological interaction scenarios. These scenarios offer an alternative to the conventional dark energy model and potentially address the Hubble tension. The assessment of these models in light of current cosmological data enables us to impose constraints on parameters.

The structure of the paper is as follows: Thermodynamic processes in relation to cosmological fluids are covered in Section II. In Section III, various cosmological scenarios are introduced to examine the Hubble tension, along with the modified Friedmann, acceleration and continuity equations based on Section II. Section IV examines the data and the statistical technique used for data analysis. Section V presents the findings and Section VI provides the final conclusion and a summary of the article.

## II. REVERSIBLE AND IRREVERSIBLE PROCESSES

We consider a spatially flat, homogeneous, and isotropic universe that functions as an open thermodynamic system characterized by a specific volume  $V = V(t)$  and a defined particle number  $N = N(t)$ . Within this framework, we posit the occurrence of matter creation in the universe coupled with an energy exchange between the bulk and its boundary. Under these conditions, the first law of thermodynamics can be expressed as

$$\frac{d}{dt}(\epsilon V) + (p + p_c) \frac{dV}{dt} = \frac{dQ}{dt}, \quad (2.1)$$

where the internal energy is denoted by  $E = \epsilon V$ , the energy density is represented by  $\epsilon = \rho c^2$  that incorporates the speed of light  $c$ , and the thermodynamic pressure is indicated by  $p$ . The creation pressure for adiabatic matter creation is introduced in [31] as

$$p_c = -\frac{(\epsilon + p)V\Gamma(t)}{\dot{V}}. \quad (2.2)$$

Here, the rate of matter creation is specified by  $\Gamma(t)$ , which is associated with  $\dot{n} + 3\frac{\dot{a}}{a}n = n\Gamma(t)$ , along with the number density of particles  $n = N/V$ .  $\Gamma(t) > 0$  corresponds to matter creation, while  $\Gamma(t) < 0$  corresponds to annihilation. On the right-hand side of equation (2.1), the heat flow  $dQ_{rev} = TdS_{rev}$  across the

horizon is delineated, leading to a total entropy change  $dS = dS_{rev} + dS_{irr}$  with  $dS_{irr} \geq 0$ , where  $S_{rev}$  and  $S_{irr}$  correspond to reversible and irreversible entropies. Furthermore, we assume an isothermal quasistatic process for energy exchange between the bulk and the horizon; therefore, the temperature at the horizon, matches the bulk temperature. We use  $dQ_{rev} = T_h dS_m$ , with an approximate Hawking temperature  $T_h = \hbar c / (2\pi k_B L)$ , where  $\hbar$  represents the reduced Planck constant and we consider the boundary as the Hubble horizon  $L = c/H$  with the Hubble function  $H$ . In addition to this, we use our recently introduced generalized horizon entropy [59]  $S_m$  based on generalized mass to horizon relation, defined as

$$S_m = \frac{2\pi k_B m \gamma}{(m+1)l_p^2} L^{m+1}, \quad (2.3)$$

with  $m$  as a nonnegative real number,  $\gamma$  a free positive parameter with dimensions of  $[length]^{1-m}$ ,  $l_p$  as Planck length, and  $k_B$  as the Boltzmann constant. Using  $V(t) = \frac{4}{3}\pi L^3$ ,  $S_m$ , and  $T_h$ , the first law (2.1) is reformulated as

$$\dot{\rho} + 3H \left( \rho + \frac{p_{eff}}{c^2} \right) = - \left( \frac{3\gamma m c^{m-1}}{4\pi G} \right) H^{2-m} \dot{H}, \quad (2.4)$$

where effective pressure  $p_{eff} = p + p_c$  is introduced with the definition of creation pressure  $p_c$ . Indeed, this equation represents a generalization of the continuity equations examined in the framework of matter creation cosmologies [60, 61], through the incorporation of energy transfer from the bulk to the horizon. The role of  $\gamma$  is to quantify this energy flow. Moreover, the aforementioned equation pertains to a single fluid model with the creation of that specific fluid. However, scenarios involving multiple fluids with distinct matter creation rates for each fluid or for one of them exclusively can also be envisaged. In the subsequent section, we will explore scenarios involving multiple fluids, considering matter creation for all fluids or for only a single fluid, alongside the energy exchange among fluid species as quantified by  $\gamma$ .

We wish to address the topic of generalized horizon entropy  $S_m$ . For comprehensive details and justifications, see our recent articles [59, 62, 63]. Traditionally, the association between entropy and temperature on horizons has been established through Bekenstein entropy, which is proportional to the horizon area and is characterized by the Hawking temperature, defined in terms of surface gravity. Various generalizations have been proposed, such as Tsallis-Cirto [64] (based on Tsallis nonextensive statistics), Barrow [65] (inspired by fractal horizons), and Rényi [66] (motivated from quantum information theory). These, however, reveal inconsistencies with the Hawking temperature when examined under the holographic principle [62, 63]. To address this issue, we have introduced a novel generalized entropy  $S_m$  [59], derived from a generalized mass-to-horizon relation

$$M = \gamma \frac{c^2}{G} L^m \quad (2.5)$$

and the Hawking temperature  $T_h$ , employing the Clausius relation. This entropy reduces to the Bekenstein entropy under certain conditions  $\gamma = m = 1$ , and  $m$  can also be rescaled to align with other nonstandard entropies, such as Barrow and Tsallis-Cirto. Notably,  $S_m$  maintains thermodynamic consistency with  $T_h$  when utilized in conjunction with the generalized mass-to-horizon relation. The generalized mass to horizon relation plays very important role in order to have thermodynamic consistency, therefore one should modify this relation to use Hawking temperature with any other nonstandard entropy. For example, for Tsallis-Cirto and Barrow entropies, one must rescale  $m$  with Tsallis-Cirto and Barrow parameters as suggested in [59].

### III. MODIFIED FRIEDMANN EQUATIONS

We consider a spatially flat Friedmann–Lemaître–Robertson–Walker (FLRW) metric  $g_{\mu\nu}$  and present a modified energy-momentum tensor  $\tilde{T}_{\mu\nu}$  of the following form  $\tilde{T}_{\mu\nu} = T_{\mu\nu} - \frac{\Lambda_{\text{rev}}(t)}{8\pi G} g_{\mu\nu}$ . This tensor accounts for changes brought about by matter creation and energy transfer across the cosmological horizon.  $T_{\mu\nu}$  comprises the standard isotropic pressure,  $p$ , of a perfect fluid as well as an extra creation pressure,  $p_c$ , associated to matter creation. Moreover, a time-dependent cosmological term,  $\Lambda_{\text{rev}}(t)$ , represents the influence of reversible energy flow and is driven by the energy exchange between the bulk and the horizon. The divergence of the modified energy-momentum tensor,  $\tilde{T}_{\mu\nu}$ , inevitably leads to a continuity equation with the definition of  $\Lambda_{\text{rev}}(t)$  coming from the right side of equation (2.4). The modified energy-momentum tensor  $\tilde{T}_{\mu\nu}$  thus describes a thermodynamic open system that is expanding nonadiabatically, including the creation of matter and the transfer of energy from the bulk to the horizon. For a multi-fluid scenario, we obtain the modified Friedmann and acceleration equations by solving the Einstein field equations as follows:

$$H^2 = \frac{8\pi G}{3} \sum_i \rho_i + \frac{8\pi G}{3} \rho_e \quad (3.1)$$

$$\frac{\ddot{a}}{a} = -\frac{4\pi G}{3} \sum_i \left( \rho_i + \frac{3p_{\text{eff},i}}{c^2} \right) + \frac{8\pi G}{3} \rho_e, \quad (3.2)$$

$$\sum_i \left[ \dot{\rho}_i + 3H \left( \rho_i + \frac{p_{\text{eff},i}}{c^2} \right) \right] = -\dot{\rho}_e, \quad (3.3)$$

where the index  $i$  runs for the total matter and radiation and we introduce the effective entropic dark energy density

$$\rho_e = \frac{3}{8\pi G} \left( \frac{2m\gamma}{3-m} c^{m-1} H^{3-m} \right) + c_0, \quad (3.4)$$

where  $c_0$  is an integration constant. It is noteworthy that the aforementioned set of equations effectively integrates the matter creation cosmologies [60, 61] with the

energy flow cosmologies [51], as governed by the matter creation function  $\Gamma(t)$  and the energy flow parameter  $\gamma$ . In the case of  $\Gamma(t) = \gamma = 0$ , these equations simplify to those represented by the standard  $\Lambda$ CDM model. It should be emphasized that these equations possess a high degree of generality concerning matter creation scenarios and energy flux. For instance, one might consider gravitationally induced adiabatic dark matter creation while all other species adhere to the standard continuity equations. Additionally, one may contemplate the adiabatic creation of all species of the universe with different creation rate functions. Intriguingly, scenarios involving solely matter creation in the absence of energy flow, as addressed by  $\Gamma(t) > 0$  for  $\rho + p > 0$ , elicit a negative creation pressure, which might account for the current accelerated expansion of the universe. However, the data will tell us about the sign of  $\Gamma(t)$ .

We shall subsequently employ  $m = 1$  in conjunction with a phenomenological function corresponding to  $\Gamma(t) = \Gamma_0 H$ . Our aim is to preserve the definition of the standard Bekenstein entropy, i.e. for  $m = 1$ . For nonstandard entropies as discussed in the preceding section, such as the Tsallis-Cirto entropy [64] and the Barrow entropy [65], a variety of parameterizations may be adopted for  $m$  [59]. Furthermore, alternative functional forms may be ascribed to  $\Gamma(t)$  [44, 47]. The aforementioned selection of  $\Gamma(t)$  has been employed in the literature due to its simplicity, however, extending beyond this function is not within the scope of this work.

In the subsequent subsections, we examine two distinct scenarios: Firstly, those instances wherein matter and radiation are impacted by the creation rate function, with energy being transferred from radiation and matter to the effective entropic dark energy. Secondly, we focus solely on the scenario involving the creation of cold dark matter exclusively. In this context, it is presumed that baryons and radiation adhere to the standard continuity equation, with energy transferring from baryons and radiation to dark matter and, subsequently, energy flowing from all three constituents to the effective entropic dark energy.

#### Model - I

For the first consideration, the continuity equations for each constituent can be expressed as

$$\dot{\rho}_m + 3H \left( \rho_m + \frac{p_{\text{eff},m}}{c^2} \right) = 3\gamma H \left( 1 - \frac{\Gamma_0}{3} \right) \rho_m, \quad (3.5)$$

$$\dot{\rho}_r + 3H \left( \rho_r + \frac{p_{\text{eff},r}}{c^2} \right) = 4\gamma H \left( 1 - \frac{\Gamma_0}{3} \right) \rho_r, \quad (3.6)$$

$$\dot{\rho}_e = -3H\gamma \left( 1 - \frac{\Gamma_0}{3} \right) \left( \rho_m + \frac{4}{3} \rho_r \right). \quad (3.7)$$

Here, we have used  $\dot{H} = -4\pi G \left( 1 - \frac{\Gamma_0}{3} \right) \left( \rho_m + \frac{4}{3} \rho_r \right)$  in (3.3) to get above equations. In this scenario, the total matter density  $\rho_m = \rho_{dm} + \rho_b$  is composed of the densities of dark matter  $\rho_{dm}$  and baryonic matter  $\rho_b$ . As

indicated by the equations above, matter and radiation do not engage in direct interaction; instead, their interaction is mediated indirectly through effective entropic dark energy  $\rho_e$ . Nonetheless, the effective entropic dark energy interacts with both matter and radiation through the transfer of energy from these components.

We write the above continuity equations for matter and radiation as

$$\dot{\rho}_i + 3H(1 + w_{eff,i})\rho_i = 0, \quad (3.8)$$

where the effective equation of state  $w_{eff,i}$  is given by  $w_{eff,i} = \beta_i - 1$ , with  $\beta_i = \alpha(1 + w_i)$ , and the parameter  $\alpha$  is defined as

$$\alpha = (1 - \gamma)\left(1 - \frac{\Gamma_0}{3}\right). \quad (3.9)$$

Solving the above continuity equations for matter and radiation, we get  $\rho_m = \rho_{m,0}a^{-3\alpha}$ ,  $\rho_r = \rho_{r,0}a^{-4\alpha}$ . and the solution for  $\rho_e$  can be easily found as

$$\rho_e = \frac{\gamma}{1 - \gamma} \left[ \rho_{m,0} (a^{-3\alpha} - 1) + \rho_{r,0} (a^{-4\alpha} - 1) \right] + \rho_{e,0}, \quad (3.10)$$

where  $\rho_{m,0}$ ,  $\rho_{r,0}$  and  $\rho_{e,0}$  are current values at  $a = 1$ . Employing equation (3.7), we can write the equation of state  $w_e$  for the effective entropic dark energy.

$$w_e = -1 + \gamma \left(1 - \frac{\Gamma_0}{3}\right) \frac{H_0^2 \Omega_{m,0} a^{-3\alpha} + \frac{4}{3} \Omega_{r,0} a^{-4\alpha}}{H^2 \Omega_e(a)}, \quad (3.11)$$

where we have introduced the dimensionless density parameters  $\Omega_i(a) = \frac{8\pi G}{3H^2(a)}\rho_i(a)$  with the present value defined at  $a = 1$ , i.e.,  $\Omega_{i,0} = \frac{8\pi G}{3H_0^2}\rho_{i,0}$ . Now, the modified continuity equation for  $\rho_e$  becomes

$$\dot{\rho}_e + 3H(1 + w_e)\rho_e = 0. \quad (3.12)$$

Then, employing  $\rho_m$ ,  $\rho_r$  and  $\rho_e$  in equation (3.1), the normalized Friedmann equation reads as

$$\frac{H^2}{H_0^2} = 1 + \frac{1}{1 - \gamma} \left[ \Omega_{m,0} (a^{-3\alpha} - 1) + \Omega_{r,0} (a^{-4\alpha} - 1) \right], \quad (3.13)$$

where we have used  $\Omega_{m,0} + \Omega_{r,0} + \Omega_{e,0} = 1$ .

## Model - II

In the second scenario, we examine a situation in which energy is transferred from radiation and baryons to dark matter, in addition to the adiabatic creation of dark matter. Additionally, we postulate the transfer of energy from dark matter, baryonic matter, and radiation to effective entropic dark energy, thereby establishing an interaction between effective entropic dark energy and all constituents. In this context, we assume that radiation

and baryons adhere to the standard continuity equations governed by  $\rho_b = \rho_{b,0}a^{-3}$  and  $\rho_r = \rho_{r,0}a^{-4}$ . The continuity equations for  $\rho_{dm}$  and  $\rho_e$  are given by

$$\dot{\rho}_{dm} + 3H \left( \rho_{dm} + \frac{P_{eff,dm}}{c^2} \right) = -\dot{\rho}_e, \quad (3.14)$$

$$\dot{\rho}_e = -3\gamma H \left( \left(1 - \frac{\Gamma_0}{3}\right) \rho_{dm} + \rho_b + \frac{4}{3} \rho_r \right) \quad (3.15)$$

where  $\dot{\rho}_e = 3\gamma H \dot{H} / (4\pi G)$  is applicable under this scenario, with  $\dot{H} = -4\pi G \left( \left(1 - \frac{\Gamma_0}{3}\right) \rho_{dm} + \rho_b + \frac{4}{3} \rho_r \right)$ . We can easily find the exact solutions for  $\rho_{dm}$  and  $\rho_e$ , by solving the above differential equations and the solution for dark matter  $\rho_{dm}$  reads as

$$\rho_{dm} = \rho_{dm,0} a^{-3\alpha} + \frac{\gamma}{\alpha - 1} \rho_{b,0} (a^{-3} - a^{-3\alpha}) + \frac{4\gamma}{3\alpha - 4} \rho_{r,0} (a^{-4} - a^{-3\alpha}). \quad (3.16)$$

and for the effective entropic density  $\rho_e$ , it gives

$$\rho_e = \rho_{e,0} + \frac{\gamma}{1 - \gamma} \left[ (a^{-3\alpha} - 1) \rho_{dm,0} + \left( (1 - \gamma) a^{-3} + \gamma \left( \frac{\alpha a^{-3} - a^{-3\alpha}}{\alpha - 1} \right) - 1 \right) \rho_{b,0} + \left( (1 - \gamma) a^{-4} + \gamma \left( \frac{3\alpha a^{-4} - 4a^{-3\alpha}}{3\alpha - 4} \right) - 1 \right) \rho_{r,0} \right]. \quad (3.17)$$

Furthermore, we write the effective equation of state  $w_e$  for entropic dark energy in this scenario as well, which reads as

$$w_e = -1 + \gamma \left[ \frac{\left(1 - \frac{\Gamma_0}{3}\right) \Omega_{dm}(a)}{\Omega_e(a)} + \frac{H_0^2 \Omega_{b,0} a^{-3} + \frac{4}{3} \Omega_{r,0} a^{-4}}{H^2 \Omega_e(a)} \right]. \quad (3.18)$$

The normalized Friedmann equation for this case can be written as

$$\frac{H^2}{H_0^2} = 1 + \frac{1}{1 - \gamma} \left[ \Omega_{dm,0} (a^{-3\alpha} - 1) + \Omega_{b,0} \left( \frac{-3\gamma a^{-3\alpha} - (1 - \gamma)\Gamma_0 a^{-3}}{3(\alpha - 1)} - 1 \right) + \Omega_{r,0} \left( \frac{-4\gamma a^{-3\alpha}}{3\alpha - 4} - \frac{(1 - \gamma)(1 + \Gamma_0)a^{-4}}{3\alpha - 4} - 1 \right) \right], \quad (3.19)$$

where we have used  $\Omega_{m,0} + \Omega_{r,0} + \Omega_{e,0} = 1$  with the definition  $\Omega_{m,0} = \Omega_{dm,0} + \Omega_{b,0}$ .

## IV. DATASETS AND METHODOLOGY

The aforementioned models will be evaluated in comparison with the most recent set of geometrical cosmological data available, to the best of our knowledge. This includes Type Ia Supernovae (SNeIa), Cosmic Chronometers (CC); the data from the Gamma Ray Bursts (GRBs);

Baryon Acoustic Oscillations (BAO); as well as Cosmic Microwave Background (CMB) distance priors. The following are the details of the datasets:

**SNeIa.** We use distance moduli from 1701 light curves of 1550 spectroscopically confirmed SNeIa from the Pantheon+ sample<sup>1</sup> [6], covering the redshift range  $0.001 < z < 2.26$ . The  $\chi_{SN}^2$  is defined as  $\chi_{SN}^2 = \Delta\boldsymbol{\mu}^{SN} \cdot \mathbf{C}_{SN}^{-1} \cdot \Delta\boldsymbol{\mu}^{SN}$ , where  $\Delta\boldsymbol{\mu} = \mu_{\text{theo}} - \mu_{\text{obs}}$  is the difference between theoretical and observed values of the distance modulus for each SNeIa, and  $\mathbf{C}_{SN}$  is the total covariance matrix (statistical and systematic). The theoretical distance modulus is calculated as  $\mu_{\text{theo}}(z_{\text{hel}}, z_{HD}, \mathbf{p}) = 25 + 5 \log_{10}[d_L(z_{\text{hel}}, z_{HD}, \mathbf{p})]$ , where  $d_L$  is the luminosity distance (in Mpc),

$$d_L(z_{\text{hel}}, z_{HD}, \mathbf{p}) = (1 + z_{\text{hel}}) \int_0^{z_{HD}} \frac{c dz'}{H(z', \mathbf{p})}, \quad (4.1)$$

with  $z_{\text{hel}}$ , the heliocentric redshift;  $z_{HD}$ , the Hubble diagram redshift [67]; and  $\mathbf{p}$ , the vector of cosmological parameters. The observed distance modulus is  $\mu_{\text{obs}} = m_B - M$ , with  $m_B$  the standardized SNeIa blue apparent magnitude and  $M$  the fiducial absolute magnitude calibrated by using primary distance anchors such as Cepheids. Generally,  $H_0$  and the absolute magnitude  $M$  are degenerate with SNeIa alone, but the Pantheon+ sample includes 77 SNeIa in host galaxies where the distance moduli can be anchored by Cepheids, breaking the degeneracy and allowing separate constraints on  $H_0$  and  $M$ . Thus, the vector  $\Delta\boldsymbol{\mu}$  is

$$\Delta\boldsymbol{\mu} = \begin{cases} m_{B,i} - M - \mu_{\text{Ceph},i} & i \in \text{Cepheid hosts} \\ m_{B,i} - M - \mu_{\text{theo},i} & \text{otherwise,} \end{cases} \quad (4.2)$$

with  $\mu_{\text{Ceph}}$  as the Cepheid-calibrated host-galaxy distance from the Pantheon+ team.

**CC.** We use the measurement of Hubble parameter from cosmic chronometers [68–72], early-type galaxies which undergo passive evolution and have a characteristic feature in their spectra, from which the Hubble parameter  $H(z)$  can be measured [73–79]. The most updated sample is from [79] and spans the redshift range  $0 < z < 1.965$ .  $\chi_H^2$  is written as  $\chi_H^2 = \Delta\boldsymbol{\mathcal{H}} \cdot \mathbf{C}_H^{-1} \cdot \Delta\boldsymbol{\mathcal{H}}$  where  $\Delta\boldsymbol{\mathcal{H}} = H_{\text{theo}} - H_{\text{data}}$  is the difference between the theoretical and observed Hubble parameter and  $\mathbf{C}_H$  is the total covariance matrix calculated following [71].

**GRBs.** We incorporate the measurement of the Hubble parameter from the gamma-ray bursts “Mayflower” sample<sup>2</sup> [80], which has been calibrated in a cosmological model-independent manner and spans the specified redshift interval  $1.44 < z < 8.1$ . The  $\chi_G^2$  is defined similarly to that for SNeIa; however, we are unable to distinguish between the  $H_0$  and the absolute magnitude, necessitating a marginalization over these quantities, in accordance with [81].

**CMB.** The cosmic microwave background is examined through a compressed likelihood methodology, which utilizes the shift parameters,  $R(\mathbf{p}) \equiv \sqrt{\Omega_m H_0^2} r(z_*, \mathbf{p})/c$  and  $l_a(\mathbf{p}) \equiv \pi r(z_*, \mathbf{p})/r_s(z_*, \mathbf{p})$ , originally established in [82] and subsequently updated in [83], in accordance with the most recent data release presented in *Planck* 2018 [4]. Furthermore, the  $\chi_{CMB}^2$  is defined as  $\chi_{CMB}^2 = \Delta\boldsymbol{\mathcal{F}}^{CMB} \cdot \mathbf{C}_{CMB}^{-1} \cdot \Delta\boldsymbol{\mathcal{F}}^{CMB}$ , where the vector  $\boldsymbol{\mathcal{F}}^{CMB}$  corresponds to specific quantities in addition to the constraints on baryonic matter content  $\Omega_b h^2$  and dark matter content  $(\Omega_{m,0} - \Omega_b) h^2$ . The photon-decoupling redshift  $z_*$  [84] is determined via the most recent fitting formula from [85]. The comoving distance at decoupling, denoted as  $r(z_*, \mathbf{p})$ , is calculated utilizing the definition of comoving distance by setting  $r(z_*, \mathbf{p}) = D_M(z_*, \mathbf{p}) = \int_0^{z_*} \frac{c dz'}{H(z', \mathbf{p})}$ . Additionally,  $r_s(z, \mathbf{p}) = \int_z^\infty \frac{c_s(z')}{H(z', \mathbf{p})} dz'$  represents the comoving sound horizon at the photon-decoupling redshift  $z_*$ , where the sound speed,  $c_s(z) = c/\sqrt{3(1 + \bar{R}_b(1+z)^{-1})}$  is provided, and the baryon-to-photon density ratio parameter is specified as  $\bar{R}_b = 31500 \Omega_b h^2 (T_{CMB}/2.7)^{-4}$  and  $T_{CMB} = 2.726$  K. The sound speed,  $c_s(z)$ , requires a generalization as it is valid solely under the conditions that baryons scale  $\propto a^{-3}$  and radiation  $\propto a^{-4}$ , implying that their respective equations of state parameters  $w_i$  are 0 and 1/3. However, in the context of Model I, the continuity equations are altered via the *effective* equations of state parameters,  $w_{\text{eff},i}$ , which may deviate from typical values. The baryon-to-photon ratio is defined as  $R_b \equiv \frac{\rho_b + p_b}{\rho_\gamma + p_\gamma} = \frac{\rho_b(1+w_b)}{\rho_\gamma(1+w_\gamma)}$  which, if  $w_b = 0$  and  $w_\gamma = 1/3$ , becomes the standard  $R_b$  with  $\bar{R}_b$  and its numerical factors coming from  $\Omega_\gamma = \Omega_r/(1+0.2271 N_{\text{eff}}) \approx 2.469 \cdot 10^{-5} h^{-2}$  [86]. For Model I,  $\rho_b$  and  $\rho_r$  do not follow the standard continuity equations. As a result, we have modified the baryon-to-photon ratio,

$$R_b = \frac{(1 + w_{\text{eff},b}) \Omega_{b,0}}{(1 + w_{\text{eff},\gamma}) \Omega_{\gamma,0}} a^\alpha = \frac{3\Omega_{b,0}}{4\Omega_{\gamma,0}} (1+z)^{-\alpha}. \quad (4.3)$$

Naturally, early-time physics is substantially and robustly constrained by a multitude of observational probes, and it is recognized that modifications within this regime could potentially result in highly unconventional outcomes. However, our approach transcends mere theoretical qualitative assertions; we intend to empirically evaluate these equations through direct data analysis. Consequently, any constraints that emerge will be statistically interpreted concerning their consistency with the equations.

**BAO.** For the analysis of baryon acoustic oscillations, we utilize data sets derived from the latest BAO measurements conducted through the dark-energy spectroscopic instrument (DESI-DR2)[8]. These measurements are based on data from Bright Galaxies, Luminous Red Galaxies, Emission Line Galaxies, Quasars and Lyman- $\alpha$  Forest, as shown in Table IV of Ref. [8]. They cover an effective redshift range from approxi-

<sup>1</sup> <https://github.com/PantheonPlusSH0ES/DataRelease>

<sup>2</sup> see Table 3 of [80]

mately  $z \approx 0.1\text{--}4.2$ . The analyses consider the transverse comoving distance  $D_M(z, \mathbf{p})/r_s(z_d, \mathbf{p})$ , the Hubble distance  $D_H/r_s(z_d, \mathbf{p})$ , and the angle-averaged distance  $D_V/r_s(z_d, \mathbf{p})$ , each standardized to the comoving sound horizon at the drag epoch,  $r_s$ . The correlations between the measurements  $D_M/r_s$  and  $D_H/r_s$  are taken into account in the calculations. The drag epoch redshift  $z_d$  [84] is determined using the latest fitting formulae from [85]. The  $\chi_{BAO}^2$  is defined as  $\chi_{BAO}^2 = \Delta \mathcal{F}^{BAO} \cdot \mathbf{C}_{BAO}^{-1} \cdot \Delta \mathcal{F}^{BAO}$  with the observables  $\mathcal{F}^{BAO}$  corresponds to  $D_M(z, \mathbf{p})/r_s(z_d, \mathbf{p})$ ,  $D_H/r_s(z_d, \mathbf{p})$ , and  $D_V/r_s(z_d, \mathbf{p})$  with  $D_V(z, \mathbf{p}) = [cz(1+z)^2 D_A^2(z, \mathbf{p})/H(z, \mathbf{p})]^{1/3}$  and  $D_A$  is the angular diameter distance defined as  $D_A = D_M/(1+z)$ .

The total  $\chi^2$  is minimized using the publicly available sampler [87], `emcee`<sup>3</sup>, which employs a pure-Python implementation of the affine invariant Markov chain Monte Carlo (MCMC) method. To evaluate the convergence and sampling efficiency of our MCMC analysis, we adhere to the recommendations given in [87, 88]. Specifically, we employ the integrated autocorrelation time ( $\tau$ ) to estimate the effective number of independent samples within our chains. This metric considers the correlation among successive samples in a Markov chain and provides a quantitative assessment of the Monte Carlo error in estimated quantities. Furthermore, we utilize trace plots to visually inspect the stability and mixing of walkers, and evaluate the acceptance fraction to determine sampler efficiency, ensuring it falls within the ideal range 0.2–0.5.

We adopt uniform priors on the model parameters within physically motivated bounds:  $0 < \Omega_{b,0} < \Omega_{m,0} < 1$ ,  $0 < h$ ,  $M < 0$ ,  $0 < \gamma$ , and  $-10 < \Gamma < 10$ . To sample the posterior distribution, we use the number of walkers,  $n_{\text{walkers}} = 50$ , chosen to be at least three times the number of model dimensions. The chains are initialized with a burn-in phase of 3000 steps, followed by 10000 steps used for the final analysis. To improve sampling efficiency and maintain a suitable acceptance fraction, we use a mixture of proposal moves: for example, a mixture of `StretchMove`, `DEMove`, and `KDEMove`. For more details, see [87] and official documentation of `emcee`.

We use `Dynesty`<sup>4</sup>[89], a nested sampling algorithm, to compute the *Bayesian evidence* for cosmological model comparison. The *Bayesian evidence*, denoted as  $\mathcal{Z}$ , is defined as the integral of the likelihood over the prior:  $\mathcal{Z} = \int \mathcal{L}(\theta) \pi(\theta) d\theta$ , where  $\mathcal{L}(\theta)$  is the likelihood and  $\pi(\theta)$  is the prior probability distribution of the parameters  $\theta$ . To compare two models,  $\mathcal{M}_1$  and  $\mathcal{M}_2$ , we compute the *Bayes factor*:  $B_{12} = \frac{\mathcal{Z}_1}{\mathcal{Z}_2}$ , natural logarithm of Bayes factor,  $\ln B_{12} = \ln \mathcal{Z}_1 - \ln \mathcal{Z}_2$ . We interpret  $\ln B_{12}$  using the Jeffreys scale [90]: This provides a statistically robust and widely accepted framework for testing extensions to the standard  $\Lambda$ CDM

model. For the comparison, we consider  $\mathcal{M}_1 = \Lambda$ CDM. Furthermore, we employ the publicly accessible Python package [91] `GetDist`<sup>5</sup> to generate plots and perform statistical analysis.

## V. RESULTS AND DISCUSSION

The main results are given in Table I. It provides 68% confidence level constraints for each parameter across three models, corresponding to dataset combinations of SNeIa, CMB distance priors, BAO, CC, and GRB. In this way, Figure 1 depicts the combined contour plots for each model parameters and standard  $\Lambda$ CDM parameters. A comparative analysis of Models I, II, and  $\Lambda$ CDM reveals distinct parameter trends that elucidate their capacity to address the Hubble tension. Models I and II, which incorporate the additional parameters  $\Gamma_0$  and  $\gamma$  representing matter creation/annihilation and energy flow, yield higher  $H_0$  values in comparison to  $\Lambda$ CDM, thereby reducing the tension, with the latest SH0ES measurements reported in 2024 [19], to a range of 1.2–1.8 $\sigma$ . Notably, upon consideration of SH0ES measurements from 2021 and 2022 [17, 18], these models further diminish the tension to around 1 $\sigma$ . These models accomplish this by employing lower matter density and baryon density, along with non-zero  $\Gamma_0$  values and stringent constraints on  $\gamma$ . Model I demonstrates a marginal advantage over Model II in mitigating the Hubble tension. Its value,  $h = 0.7173 \pm 0.0079$ , is more closely aligned with the latest SH0ES measurement,  $h = 0.7317 \pm 0.0086$ , thus reducing the discrepancy to  $\sim 1.2\sigma$  and Model II persists at an approximate 1.8 $\sigma$ . Moreover, the more pronounced negative value of  $\Gamma_0$  in Model I, in comparison to that in Model I, suggests more significant modifications to the late-time cosmic expansion. This is accompanied by smaller values of  $\gamma$ , which serves to quantify a very small energy transfer towards the effective dark entropic dark energy. Both  $\Gamma_0$  and  $\gamma$  are crucial in altering the late-time expansion history of the universe, resulting in elevated values of  $H_0$  for both models, compared to  $\Lambda$ CDM.

An analysis of Figure 2 illustrates the evolution of dimensionless density parameters for Model I. Prior to recombination, it is observed that the total matter (depicted in orange) surpasses the  $\Lambda$ CDM, while baryonic matter (illustrated in green) and radiation (in red) are comparatively less. This is evident because they diverge from standard continuity equations due to matter creation functions and interactions with effective entropic dark energy, as energy transfers from matter and radiation to effective entropic dark energy. In the post-recombination era, an energy transfer from total matter and radiation to effective entropic dark energy becomes evident, as all dimensionless density parameters diminish except for the effective entropic dark energy, which

<sup>3</sup> <https://github.com/dfm/emcee>

<sup>4</sup> <https://dynesty.readthedocs.io/en/v2.1.5/>

<sup>5</sup> <https://github.com/cmbant/getdist>

Parameter	Model-I	Model-II	$\Lambda$ CDM
$\Omega_{m,0}$	$0.286 \pm 0.004$	$0.283 \pm 0.005$	$0.293 \pm 0.004$
$\Omega_{b,0}$	$0.044 \pm 0.0008$	$0.045 \pm 0.0008$	$0.047 \pm 0.0004$
$h$	$0.717 \pm 0.008$	$0.711 \pm 0.008$	$0.689 \pm 0.003$
$\gamma$	$< 0.0343$	$< 0.0029$	—
$\Gamma_0$	$-0.044^{+0.038}_{-0.015}$	$-0.021^{+0.011}_{-0.005}$	—
$\mathcal{M}$	$-19.312 \pm 0.023$	$-19.334 \pm 0.023$	$-19.398 \pm 0.009$
$\ln \mathcal{Z}_i$	$-836.773 \pm 0.108$	$-837.735 \pm 0.105$	$-832.494 \pm 0.089$
$\ln B_{\Lambda\text{CDM},i}$	$4.279 \pm 0.140$	$5.241 \pm 0.137$	0

Table I: Marginalized median values and 68% confidence intervals for cosmological parameters for each model. For  $\gamma$ , the 95% upper confidence limit is reported where the constraint is weak. The table also includes the *Bayesian evidence* and *Bayes factors* for each model.

remains substantially large. At this juncture, the quantity of effective entropic dark energy exceeds that of the  $\Lambda$ CDM, indicating a late-time modification of the expansion rate. This observation is further substantiated by an initial positive deviation concerning matter, transitioning to a negative deviation following recombination. Moreover, effective entropic dark energy exhibits a very high positive deviation during the latter period, highlighting late-time modifications in the expansion rate, which in turn addresses the Hubble tension.

Upon examining Figure 3, the behavior of the dimensionless density parameters compared to the  $\Lambda$ CDM model presents notable insights. Model II, as opposed to Model I, initially exhibits higher baryonic matter and radiation relative to the standard  $\Lambda$ CDM model. Prior to recombination, baryonic matter and radiation display a precipitous decline, indicating a rapid transfer of energy from baryonic matter and radiation to dark matter, particularly pronounced around the recombination epoch. Following recombination, there is an observed transition of energy flow from dark matter, baryonic matter, and radiation to effective entropic dark energy. Analyzing the percentage deviation, dark matter demonstrates a sharp positive deviation around recombination, and this deviation decreases and crosses a late-time negative deviation, which is counterbalanced by an increase in effective dark energy at later times. This reflects a modification in the expansion rate after recombination and during very later times, thereby supporting this model's potential to address the Hubble tension.

For both models, the parameters  $\gamma$  and  $\Gamma_0$  play a significantly influential role. The parameter  $\gamma$  governs the distribution of energy among various species in the universe. In both models, the relatively small value of  $\gamma$  indicates that the effective entropic dark energy functions as a slowly varying cosmological constant. Notably, for both models, the data suggest a negative value for  $\Gamma_0$ , which implies the annihilation or decay of species. For

model I, where the creation/annihilation of all species is considered in addition to energy flow from all species to effective entropic dark energy, the negative value of  $\Gamma_0$  implies data prefers annihilation, therefore, in addition to slow energy flow quantified by  $\gamma$ ; the matter annihilation play the important role to modify the late time expansion, showing more effective entropic dark density. Note that, as [44] states,  $\Gamma(t) < 0$  alone is insufficient to account for accelerated expansion unless a new fluid with a negative equation of state is introduced. Our findings support this assertion, as the effective entropic dark energy, through the energy transfer from the bulk to the horizon, assumes the role of this new fluid. This phenomenon suggests that the energy flow, quantified by  $\gamma$ , along with the negative decay rate  $\Gamma(t) = \Gamma_0 H(t)$ , is crucial for modifying the universe's late-time accelerating expansion, thereby validating both models in addressing the Hubble tension.

The parameters  $\gamma$  and  $\Gamma_0$  exhibit a strong correlation mediated by the effective scaling parameter  $\alpha = (1 - \gamma)(1 - \Gamma_0/3)$ , as represented in the continuity equations. Constraints on  $\alpha$  are given by  $\alpha = 1.00129 \pm 0.00042$  for Model I, and by  $\alpha = 1.0046^{+0.0013}_{-0.0015}$  at  $1\sigma$  for Model II. In Model I, a minor change in the scaling parameter ( $\alpha > 1$ ) leads to a reduced sound horizon ( $r_s(z_*) = 140.18 \text{ Mpc}$ ,  $r_s(z_d) = 142.56 \text{ Mpc}$ ) compared to  $\Lambda$ CDM ( $r_s(z_*) = 145.45 \text{ Mpc}$ ,  $r_s(z_d) = 148.04 \text{ Mpc}$ ), enabling a slight increase in  $H_0$ . The change in the baryon-to-photon ratio,  $R_b \propto (1+z)^{-1.00129}$ , slightly enhances the early universe's sound speed, but the the Hubble function dominates due to the early time behavior of the effective energy density,  $\rho_e$ , and thermodynamic interactions, to overcome the slight increment in the sound speed. In Model II, while the photon-to-baryon ratio is unchanged, the sound horizon reduction stems from interactions among radiation, baryons and dark matter, and early time behavior of the effective entropic dark energy.

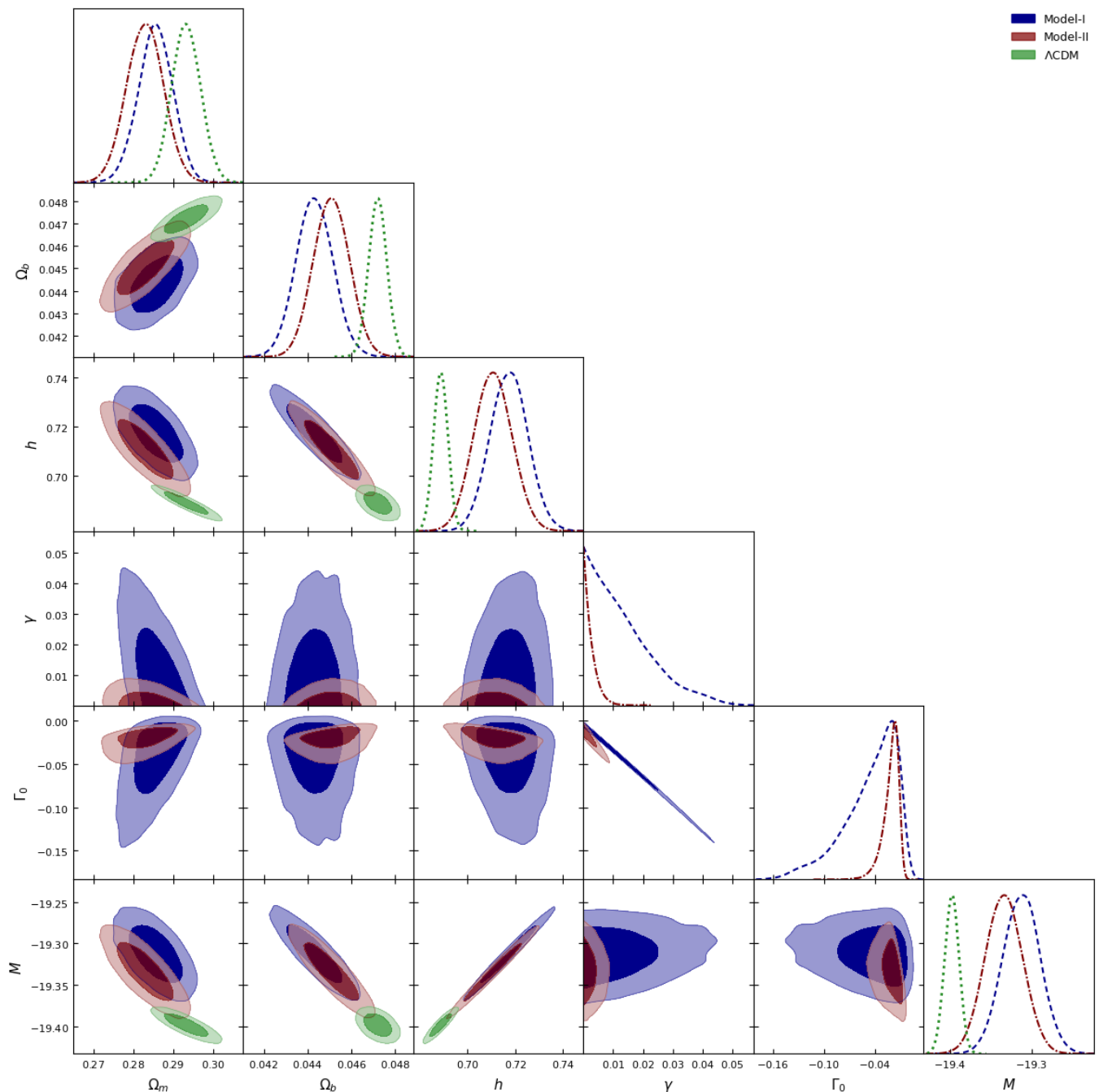


Figure 1: Contour plots represent 68% and 95% confidence regions for each model, allowing a comparison of deviations between them.

An important aspect of these models is the behavior of the effective equation of states with respect to the effective entropic dark energy. As shown in Figure 4, it starts exhibiting traits similar to radiation and transitions around the recombination era. Around  $a = 0.01$ , it further evolves to display dust-like characteristics. Afterwards, it behaves akin to quintessence, ultimately reaching the value of the cosmological constant today. In both models, the assumed scenarios for entropic dark energy

undergo changes depending on the different evolutionary stages of the universe, presenting a coherent scenario that extends from the matter and radiation sectors to the dark sector. This behavior is particularly evident in Chaplygin gas cosmological models [92, 93], running vacuum models [94] and certain scalar-tensor gravity models [95], where a single fluid initially mimics dark matter, eventually transitioning to represent dark energy fluids. Thus, both dark matter and dark energy might be two manifes-

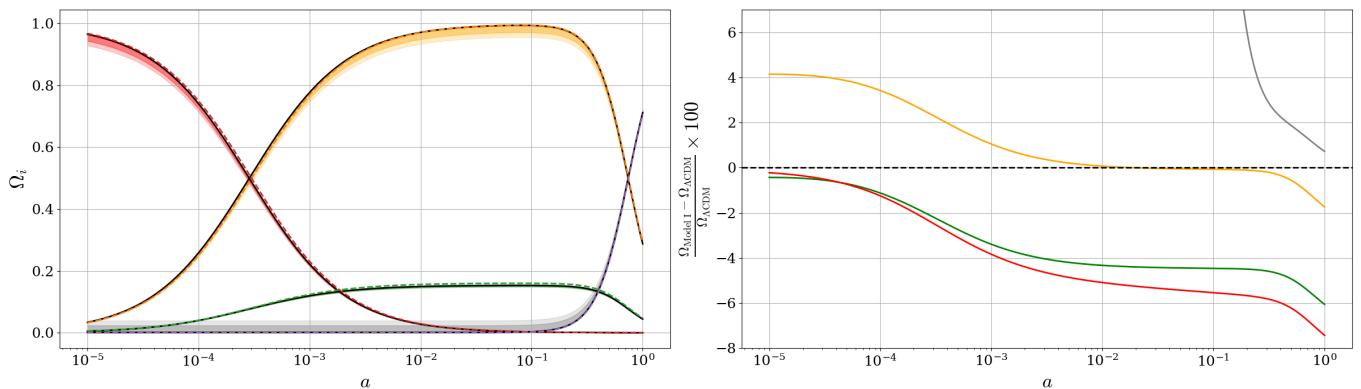


Figure 2: Evolution of the dimensionless density parameters,  $\Omega_i(a)$  with  $1\sigma$  and  $2\sigma$  confidence regions shown as shaded areas and percent deviation of  $\Omega_i$  relative to the standard  $\Lambda$ CDM, as a function of the scale factor  $a$  for Model-I. The dashed lines represent the  $\Lambda$ CDM model, and the black lines correspond to the dimensionless density parameters evaluated at the best fit values for Model-I. Orange color for total matter (dark matter plus baryonic matter), green for baryonic matter, red for radiation and gray for effective dark entropic dark energy

tations of the same underlying entity. Specifically, in our framework, the effective entropic dark energy imitates not only early dark matter but also radiation before transitioning to the cosmological constant in the current era. In both models, this behavior is responsible for modifying the early physics around recombination, in addition to the energy flow among different constituents considered in these thermodynamic interacting scenarios.

Interestingly, while both models are mathematically equivalent to running vacuum models [96] considering  $\Gamma_0 = 0$ , the underlying physical mechanisms of both approaches differ substantially. The constraints on  $\gamma \approx 10^{-3} - 10^{-2}$  derived from our analysis correspond to the parameter  $\nu$ , which characterizes the running of vacuum energy and is of a similar order of magnitude. Additionally, constraints on  $\gamma$  in our generalized entropic force models [62] yield equivalent values for this parameter. Consequently, the constraints on  $\Gamma_0$  within the cosmological model of the entropic force [47] are consistent with our analysis. Lastly, examining the Bayesian evidence based on Jeffreys scale and looking at Table 1, the data shows strong preference for  $\Lambda$ CDM over both models.

## VI. CONCLUSION

We have proposed a new approach to address the Hubble tension by incorporating thermodynamic processes, thus modifying the evolution equations to explore thermodynamically interacting cosmological models. We analyzed two scenarios involving gravitationally induced adiabatic matter creation with the energy transfer from the bulk to the cosmological horizon. The first scenario examines the creation of matter across all species, accompanied by a transfer of energy from matter and radiation to an effective entropic dark energy. The second scenario focuses on a situation where solely dark mat-

ter is subjected to creation or annihilation, with energy being transferred from baryonic matter and radiation to dark matter. Furthermore, the second scenario examines the energy transfer to effective entropic dark energy from the total matter and radiation. These considerations modify the expansion rate at early and late times through an augmented presence of effective entropic dark energy due to energy transfer from bulk to the horizon, thereby addressing the Hubble tension.

This study integrates matter creation cosmologies with energy flow cosmologies into a unified framework, offering an alternative approach to comprehending the accelerated expansion of the universe, and in particular, addressing the Hubble tension. It provides novel avenues for examining interacting cosmological fluid scenarios from a thermodynamic viewpoint by employing the first and second laws of thermodynamics, demonstrating that these integrated scenarios address the challenges encountered by the standard  $\Lambda$ CDM model.

The matter creation/annihilation functions,  $\Gamma(t)$ , the specification of chosen horizon entropy,  $S_m$ , together with the associated horizon temperature,  $T_h$ , are pivotal in both scenarios. While this analysis employed a specific phenomenological creation function,  $\Gamma(t) = \Gamma_0 H$ , exploring additional functions would be advantageous for achieving a more profound understanding. Instances include functions such as  $\Gamma(t) = \Gamma_0$ ,  $\Gamma_0 + \Gamma_1 H$ ,  $\Gamma_0 + \Gamma_1 H + \Gamma_2 H^2$ , among others. Consequently, this study has been confined to Bekenstein entropy,  $m = 1$ . Nonetheless, through appropriate parameterization,  $m$ , it could be extended to incorporate alternative definitions of nonstandard entropies, such as Tsallis-Cirto entropy and Barrow entropy. For thermodynamic and holographic coherence, it is imperative that the generalized horizon entropy,  $S_m$ , be adapted for Tsallis-Cirto and Barrow entropy by utilizing the generalized mass-horizon relationship. Literature indicates that nonstandard entropies have some-

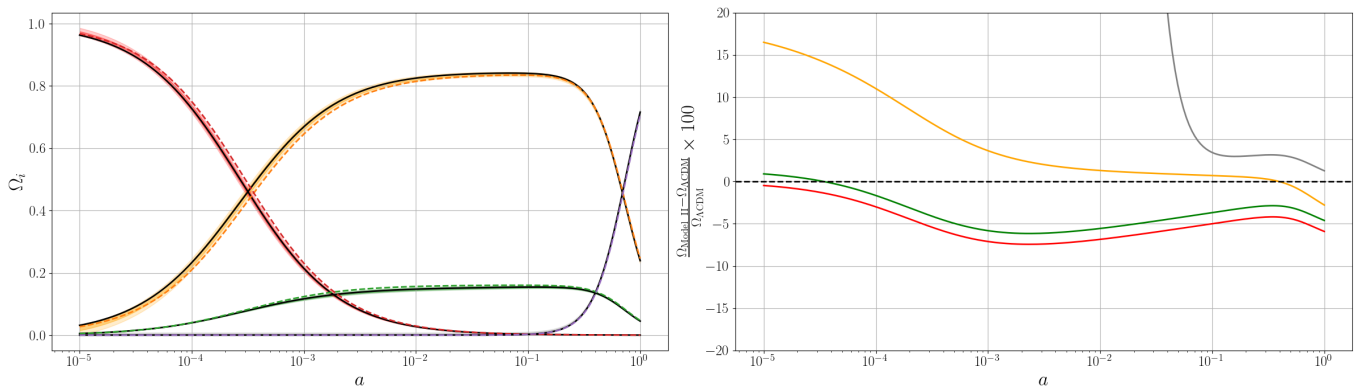


Figure 3: Evolution of the dimensionless density parameters  $\Omega_i(a)$  and percent deviation of  $\Omega_i(a)$  in Model II relative to the standard  $\Lambda$ CDM. Here, orange color only represents the dark matter.

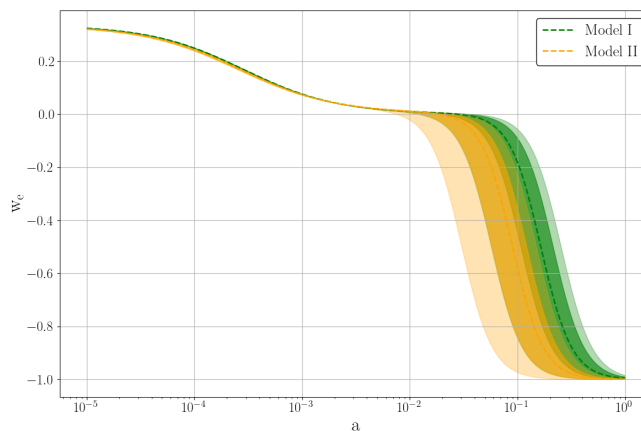


Figure 4: Evolution of effective equation of state  $w_e$  with respect to scale factor  $a$  for Model I (green) and Model II (orange). Shaded regions are  $1\sigma$  and  $2\sigma$  confidence regions and dotted lines represents the evolution on mean values.

times been inaccurately applied in cosmological contexts, and there has been an ongoing debate about the compatibility of Hawking temperature with nonstandard entropies. Hence, we adhere to the standard thermodynamic quantities defined on the Hubble horizon.

Furthermore, we have not accounted for perturbations in assessing the growth rate of structures, and a comprehensive CMB power spectrum analysis should be incorporated to fully understand the relevance of these models in addressing current cosmological challenges, particularly, the  $\sigma_8$  tension. In addition to this, more general thermodynamic interaction scenarios could be investigated within this framework. These factors will be considered

in our future work.

In conclusion, we have demonstrated that these models address the Hubble tension through straightforward modifications to the  $\Lambda$ CDM model by integrating both reversible and irreversible thermodynamic processes, thereby underscoring the significance of these thermodynamic interactions within cosmological frameworks.

#### ACKNOWLEDGMENTS

The author thanks Vincenzo Salzano for his valuable input on the data analysis part.

- 
- [1] S. Perlmutter *et al.* (Supernova Cosmology Project), *Astrophys. J.* **517**, 565 (1999), [arXiv:astro-ph/9812133](#).  
[2] A. G. Riess *et al.* (Supernova Search Team), *Astron. J.* **116**, 1009 (1998), [arXiv:astro-ph/9805201](#).  
[3] G. Hinshaw *et al.* (WMAP), *Astrophys. J. Suppl.* **208**, 19 (2013), [arXiv:1212.5226 \[astro-ph.CO\]](#).  
[4] N. Aghanim *et al.* (Planck), *Astron. Astrophys.* **641**, A6 (2020), [Erratum: *Astron. Astrophys.* 652, C4 (2021)], [arXiv:1807.06209 \[astro-ph.CO\]](#).  
[5] S. Alam *et al.* (eBOSS), *Phys. Rev. D* **103**, 083533 (2021), [arXiv:2007.08991 \[astro-ph.CO\]](#).

- [6] D. Brout *et al.*, *Astrophys. J.* **938**, 110 (2022), [arXiv:2202.04077 \[astro-ph.CO\]](#).
- [7] T. M. C. Abbott *et al.* (DES), *Phys. Rev. D* **107**, 083504 (2023), [arXiv:2207.05766 \[astro-ph.CO\]](#).
- [8] M. Abdul Karim *et al.* (DESI), (2025), [arXiv:2503.14738 \[astro-ph.CO\]](#).
- [9] L. Perivolaropoulos and F. Skara, *New Astron. Rev.* **95**, 101659 (2022), [arXiv:2105.05208 \[astro-ph.CO\]](#).
- [10] P. Bull *et al.*, *Phys. Dark Univ.* **12**, 56 (2016), [arXiv:1512.05356 \[astro-ph.CO\]](#).
- [11] W. L. Freedman, *Astrophys. J.* **919**, 16 (2021), [arXiv:2106.15656 \[astro-ph.CO\]](#).
- [12] M. Li, X.-D. Li, S. Wang, and Y. Wang, *Commun. Theor. Phys.* **56**, 525 (2011), [arXiv:1103.5870 \[astro-ph.CO\]](#).
- [13] S. Nojiri and S. D. Odintsov, *eConf C0602061*, 06 (2006), [arXiv:hep-th/0601213](#).
- [14] M. Ishak, *Living Rev. Rel.* **22**, 1 (2019), [arXiv:1806.10122 \[astro-ph.CO\]](#).
- [15] A. Arbey and F. Mahmoudi, *Prog. Part. Nucl. Phys.* **119**, 103865 (2021), [arXiv:2104.11488 \[hep-ph\]](#).
- [16] M. Cirelli, A. Strumia, and J. Zupan, (2024), [arXiv:2406.01705 \[hep-ph\]](#).
- [17] A. G. Riess, S. Casertano, W. Yuan, J. B. Bowers, L. Macri, J. C. Zinn, and D. Scolnic, *Astrophys. J. Lett.* **908**, L6 (2021), [arXiv:2012.08534 \[astro-ph.CO\]](#).
- [18] A. G. Riess *et al.*, *Astrophys. J. Lett.* **934**, L7 (2022), [arXiv:2112.04510 \[astro-ph.CO\]](#).
- [19] L. Breuval, A. G. Riess, S. Casertano, W. Yuan, L. M. Macri, M. Romaniello, Y. S. Murakami, D. Scolnic, G. S. Anand, and I. Soszyński, *Astrophys. J.* **973**, 30 (2024), [arXiv:2404.08038 \[astro-ph.CO\]](#).
- [20] N. Schöneberg, G. Franco Abellán, A. Pérez Sánchez, S. J. Witte, V. Poulin, and J. Lesgourgues, *Phys. Rept.* **984**, 1 (2022), [arXiv:2107.10291 \[astro-ph.CO\]](#).
- [21] E. Di Valentino *et al.*, *Astropart. Phys.* **131**, 102605 (2021), [arXiv:2008.11284 \[astro-ph.CO\]](#).
- [22] E. Di Valentino, O. Mena, S. Pan, L. Visinelli, W. Yang, A. Melchiorri, D. F. Mota, A. G. Riess, and J. Silk, *Class. Quant. Grav.* **38**, 153001 (2021), [arXiv:2103.01183 \[astro-ph.CO\]](#).
- [23] L. Verde, T. Treu, and A. G. Riess, *Nature Astron.* **3**, 891 (2019), [arXiv:1907.10625 \[astro-ph.CO\]](#).
- [24] E. Di Valentino *et al.*, (2025), [arXiv:2504.01669 \[astro-ph.CO\]](#).
- [25] W.-M. Dai, Y.-Z. Ma, and H.-J. He, *Phys. Rev. D* **102**, 121302 (2020), [arXiv:2003.03602 \[astro-ph.CO\]](#).
- [26] W. Yang, S. Pan, E. Di Valentino, E. N. Saridakis, and S. Chakraborty, *Phys. Rev. D* **99**, 043543 (2019), [arXiv:1810.05141 \[astro-ph.CO\]](#).
- [27] E. Di Valentino, A. Melchiorri, O. Mena, and S. Vagnozzi, *Phys. Dark Univ.* **30**, 100666 (2020), [arXiv:1908.04281 \[astro-ph.CO\]](#).
- [28] S. Kumar, R. C. Nunes, and S. K. Yadav, *Eur. Phys. J. C* **79**, 576 (2019), [arXiv:1903.04865 \[astro-ph.CO\]](#).
- [29] V. Poulin, T. L. Smith, T. Karwal, and M. Kamionkowski, *Phys. Rev. Lett.* **122**, 221301 (2019), [arXiv:1811.04083 \[astro-ph.CO\]](#).
- [30] M. Kamionkowski and A. G. Riess, *Ann. Rev. Nucl. Part. Sci.* **73**, 153 (2023), [arXiv:2211.04492 \[astro-ph.CO\]](#).
- [31] I. Prigogine, J. Geheñiau, E. Gunzig, and P. Nardone, *Gen. Rel. Grav.* **21**, 767 (1989).
- [32] J. A. S. Lima, R. Portugal, and I. Waga, *Phys. Rev. D* **37**, 2755 (1988).
- [33] J. A. S. Lima and A. S. M. Germano, *Phys. Lett. A* **170**, 373 (1992).
- [34] M. O. Calvao, J. A. S. Lima, and I. Waga, *Phys. Lett. A* **162**, 223 (1992).
- [35] J. A. S. Lima, A. S. M. Germano, and L. R. W. Abramo, *Phys. Rev. D* **53**, 4287 (1996), [arXiv:gr-qc/9511006](#).
- [36] J. S. Alcaniz and J. A. S. Lima, *Astron. Astrophys.* **349**, 729 (1999), [arXiv:astro-ph/9906410](#).
- [37] L. R. W. Abramo and J. A. S. Lima, *Class. Quant. Grav.* **13**, 2953 (1996), [arXiv:gr-qc/9606064](#).
- [38] W. Zimdahl, *Phys. Rev. D* **61**, 083511 (2000), [arXiv:astro-ph/9910483](#).
- [39] J. A. S. Lima and I. Baranov, *Phys. Rev. D* **90**, 043515 (2014), [arXiv:1411.6589 \[gr-qc\]](#).
- [40] J. F. Jesus, F. A. Oliveira, S. Basilakos, and J. A. S. Lima, *Phys. Rev. D* **84**, 063511 (2011), [arXiv:1105.1027 \[astro-ph.CO\]](#).
- [41] S. Pan, J. de Haro, A. Paliathanasis, and R. J. Slagter, *Mon. Not. Roy. Astron. Soc.* **460**, 1445 (2016), [arXiv:1601.03955 \[gr-qc\]](#).
- [42] S. Pan, J. D. Barrow, and A. Paliathanasis, *Eur. Phys. J. C* **79**, 115 (2019), [arXiv:1812.05493 \[gr-qc\]](#).
- [43] M. P. Freaza, R. S. de Souza, and I. Waga, *Phys. Rev. D* **66**, 103502 (2002).
- [44] S. Halder, J. de Haro, S. Pan, T. Saha, and S. Chakraborty, (2025), [arXiv:2502.03256 \[gr-qc\]](#).
- [45] J. Solà Peracaula and H. Yu, *Gen. Rel. Grav.* **52**, 17 (2020), [arXiv:1910.01638 \[gr-qc\]](#).
- [46] T. Harko, F. S. N. Lobo, J. P. Mimoso, and D. Pavón, *Eur. Phys. J. C* **75**, 386 (2015), [arXiv:1508.02511 \[gr-qc\]](#).
- [47] H. Gohar and V. Salzano, *Eur. Phys. J. C* **81**, 338 (2021), [arXiv:2008.09635 \[gr-qc\]](#).
- [48] K. Freese, F. C. Adams, J. A. Frieman, and E. Mottola, *Nucl. Phys. B* **287**, 797 (1987).
- [49] J. A. S. Lima and M. Trodden, *Phys. Rev. D* **53**, 4280 (1996), [arXiv:astro-ph/9508049](#).
- [50] J. M. F. Maia and J. A. S. Lima, *Phys. Rev. D* **65**, 083513 (2002), [arXiv:astro-ph/0112091](#).
- [51] J. D. Barrow and T. Clifton, *Phys. Rev. D* **73**, 103520 (2006), [arXiv:gr-qc/0604063](#).
- [52] M. Szydlowski, *Phys. Lett. B* **632**, 1 (2006), [arXiv:astro-ph/0502034](#).
- [53] M. Szydlowski, T. Stachowiak, and R. Wojtak, *Phys. Rev. D* **73**, 063516 (2006), [arXiv:astro-ph/0511650](#).
- [54] J. A. S. Lima, *Phys. Rev. D* **54**, 2571 (1996), [arXiv:gr-qc/9605055](#).
- [55] M. O. Calvao, H. P. de Oliveira, J. M. Salim, and D. Pavon, *Phys. Rev. D* **45**, 3869 (1992).
- [56] L. Parker, *Phys. Rev. Lett.* **21**, 562 (1968).
- [57] L. Parker, *Phys. Rev. D* **3**, 346 (1971), [Erratum: *Phys. Rev. D* **3**, 2546–2546 (1971)].
- [58] Y. B. Zel'dovich and A. A. Starobinsky, *JETP Lett.* **26**, 252 (1977).
- [59] H. Gohar and V. Salzano, *Phys. Rev. D* **109**, 084075 (2024), [arXiv:2307.06239 \[gr-qc\]](#).
- [60] J. A. S. Lima, R. C. Santos, and J. V. Cunha, *JCAP* **03**, 027 (2016), [arXiv:1508.07263 \[gr-qc\]](#).
- [61] J. Lima, J. Jesus, and F. Oliveira, *Journal of Cosmology and Astroparticle Physics* **2010**, 027–027 (2010).
- [62] H. Gohar and V. Salzano, *Phys. Lett. B* **855**, 138781 (2024), [arXiv:2307.01768 \[gr-qc\]](#).
- [63] I. Ćimdiker, M. P. Dąbrowski, and H. Gohar, *Eur. Phys. J. C* **83**, 169 (2023), [arXiv:2208.04473 \[gr-qc\]](#).

- [64] C. Tsallis and L. J. L. Cirto, *Eur. Phys. J. C* **73**, 2487 (2013), [arXiv:1202.2154 \[cond-mat.stat-mech\]](#).
- [65] J. D. Barrow, *Phys. Lett. B* **808**, 135643 (2020), [arXiv:2004.09444 \[gr-qc\]](#).
- [66] A. Alonso-Serrano, M. P. Dabrowski, and H. Gohar, *Phys. Rev. D* **103**, 026021 (2021), [arXiv:2009.02129 \[gr-qc\]](#).
- [67] A. Carr, T. M. Davis, D. Scolnic, D. Scolnic, K. Said, D. Brout, E. R. Peterson, and R. Kessler, *Publ. Astron. Soc. Austral.* **39**, e046 (2022), [arXiv:2112.01471 \[astro-ph.CO\]](#).
- [68] R. Jimenez and A. Loeb, *Astrophys. J.* **573**, 37 (2002), [arXiv:astro-ph/0106145](#).
- [69] M. Moresco, R. Jimenez, A. Cimatti, and L. Pozzetti, *JCAP* **03**, 045 (2011), [arXiv:1010.0831 \[astro-ph.CO\]](#).
- [70] M. Moresco, R. Jimenez, L. Verde, L. Pozzetti, A. Cimatti, and A. Citro, *Astrophys. J.* **868**, 84 (2018), [arXiv:1804.05864 \[astro-ph.CO\]](#).
- [71] M. Moresco, R. Jimenez, L. Verde, A. Cimatti, and L. Pozzetti, *Astrophys. J.* **898**, 82 (2020), [arXiv:2003.07362 \[astro-ph.GA\]](#).
- [72] M. Moresco *et al.*, *Living Rev. Rel.* **25**, 6 (2022), [arXiv:2201.07241 \[astro-ph.CO\]](#).
- [73] M. Moresco, L. Verde, L. Pozzetti, R. Jimenez, and A. Cimatti, *JCAP* **07**, 053 (2012), [arXiv:1201.6658 \[astro-ph.CO\]](#).
- [74] M. Moresco *et al.*, *JCAP* **08**, 006 (2012), [arXiv:1201.3609 \[astro-ph.CO\]](#).
- [75] M. Moresco, *Mon. Not. Roy. Astron. Soc.* **450**, L16 (2015), [arXiv:1503.01116 \[astro-ph.CO\]](#).
- [76] M. Moresco, R. Jimenez, L. Verde, A. Cimatti, L. Pozzetti, C. Maraston, and D. Thomas, *JCAP* **12**, 039 (2016), [arXiv:1604.00183 \[astro-ph.CO\]](#).
- [77] M. Moresco and F. Marulli, *Mon. Not. Roy. Astron. Soc.* **471**, L82 (2017), [arXiv:1705.07903 \[astro-ph.CO\]](#).
- [78] R. Jimenez, A. Cimatti, L. Verde, M. Moresco, and B. Wandelt, *JCAP* **03**, 043 (2019), [arXiv:1902.07081 \[astro-ph.CO\]](#).
- [79] K. Jiao, N. Borghi, M. Moresco, and T.-J. Zhang, *Astrophys. J. Suppl.* **265**, 48 (2023), [arXiv:2205.05701 \[astro-ph.CO\]](#).
- [80] J. Liu and H. Wei, *Gen. Rel. Grav.* **47** (2015), 10.1007/s10714-015-1986-1, [arXiv:1410.3960](#).
- [81] A. Conley *et al.* (SNLS), *Astrophys. J. Suppl.* **192**, 1 (2011), [arXiv:1104.1443 \[astro-ph.CO\]](#).
- [82] Y. Wang and P. Mukherjee, *Phys. Rev. D* **76**, 103533 (2007), [arXiv:astro-ph/0703780](#).
- [83] Z. Zhai, C.-G. Park, Y. Wang, and B. Ratra, *JCAP* **07**, 009 (2020), [arXiv:1912.04921 \[astro-ph.CO\]](#).
- [84] W. Hu and N. Sugiyama, *Astrophys. J.* **471**, 542 (1996), [arXiv:astro-ph/9510117](#).
- [85] A. Aizpuru, R. Arjona, and S. Nesseris, *Phys. Rev. D* **104**, 043521 (2021), [arXiv:2106.00428 \[astro-ph.CO\]](#).
- [86] E. Komatsu *et al.* (WMAP), *Astrophys. J. Suppl.* **180**, 330 (2009), [arXiv:0803.0547 \[astro-ph\]](#).
- [87] D. Foreman-Mackey, D. W. Hogg, D. Lang, and J. Goodman, *PASP* **125**, 306 (2013), 1202.3665.
- [88] J. Goodman and J. Weare, *Commun. Appl. Math. Comput. Sci.* **5**, 65 (2010).
- [89] J. S. Speagle, *Monthly Notices of the Royal Astronomical Society* **493**, 3132–3158 (2020).
- [90] H. Jeffreys, *The Theory of Probability* (Oxford Classic Texts in the Physical Sciences, 1939).
- [91] A. Lewis, (2019), [arXiv:1910.13970 \[astro-ph.IM\]](#).
- [92] C.-G. Park, J.-c. Hwang, J. Park, and H. Noh, *Phys. Rev. D* **81**, 063532 (2010), [arXiv:0910.4202 \[astro-ph.CO\]](#).
- [93] R. von Martens, D. Barbosa, and J. Alcaniz, *JCAP* **04**, 052 (2023), [arXiv:2208.06302 \[astro-ph.CO\]](#).
- [94] C. Moreno-Pulido and J. Sola Peracaula, *Eur. Phys. J. C* **82**, 1137 (2022), [arXiv:2207.07111 \[gr-qc\]](#).
- [95] A. G. Ferrari, M. Ballardini, F. Finelli, and D. Paoletti, *Phys. Rev. D* **111**, 083523 (2025), [arXiv:2501.15298 \[astro-ph.CO\]](#).
- [96] J. Solà Peracaula, J. de Cruz Pérez, and A. Gomez-Valent, *Mon. Not. Roy. Astron. Soc.* **478**, 4357 (2018), [arXiv:1703.08218 \[astro-ph.CO\]](#).